Journal of Materials Chemistry C

Accepted Manuscript

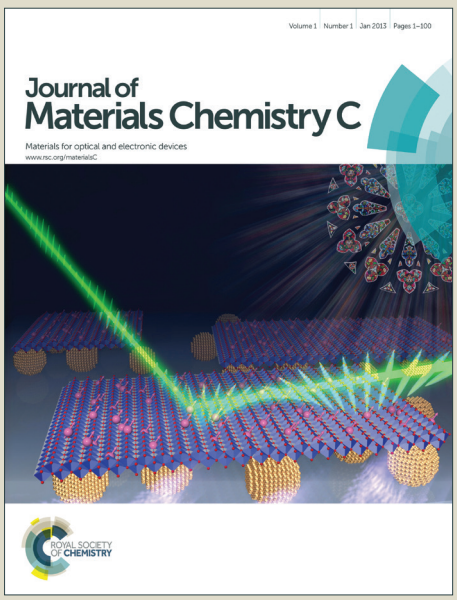

ROYAL SOCIETY OF CHEMISTRY

www.rsc.org/materialsC

Cite this: DOI: 10.1039/c0xx00000x

www.rsc.org/xxxxxx

ARTICLE TYPE

Rapid templated fabrication of large-scale, high-density metallic nanocone arrays and SERS application

Jing Zhao, Wangning Sun, Weijie Sun, Lingzhi Liu, Xiaoxiang Xia, Baogang Quang, Aizi Jin, Changzhi Gu* and Junjie Li*

Received (in XXX, XXX) Xth XXXXXXXXX 20XX, Accepted Xth XXXXXXXXX 20XX
DOI: 10.1039/b000000x

A simple and universal templating approach is developed for fabricating large-scale ordered metallic nanocone arrays with high density (5×10^8 tips cm^{-2}). A silicon nanocone array is prepared as the original template to form conical pits in a soft polymer template by thermal nanoimprinting. After metal deposition fills the pits, the resulting large-scale metallic nanocone array with sharp nanotips can be adhered to and peeled onto another polymer substrate by a simple, novel process. Avoiding the challenges of peeling from a hard template, a crucial baking process enables peeling, taking advantage of the difference in glass transition temperature (GTT) between the respective soft polymer materials of the deposition template and the transfer substrate. The method as a whole is designed for perfectible formation of a variety of metallic nanocone arrays. It provides a universally reliable shortcut to fabricate large-scale metallic nanocone arrays without lithography or etching steps, and it can be extended to the fabrication of other three-dimensional metallic-array nanostructures. Further, the as-formed Ag nanocone arrays show a large, stable surface enhancement for Raman scattering due to the nanofocused effect of electromagnetic field induced by the conical nanostructures.

Introduction

Metal nanostructures, such as arrays of nanospheres[1,2], nanosquares[3], or nanorings[4,5], as well as nanogratings[6,7], have attracted much interest due to remarkable surface plasmon polariton (SPP) resonant properties. Based on these SPP properties, an electromagnetic field can be modulated, localized or propagated – phenomena which have has been widely applied in surface enhanced Raman scattering (SERS) [8,9], molecular fluorescence [10,11], metamaterials [12,13] and other related fields of nano-optics [14,15]. At present, research on metal nanostructures has been mostly concentrated on 2D metallic nanostructures due to their simplicity and the maturity of applicable fabrication methods. Recently however, more and more 3D metallic nanostructures have been fabricated and researched due to their dimensional effects.[16] Among the many kinds of 3D metallic nanostructures, the metal nanocone is a unique nanostructure because of its special geometry and outstanding properties such as substantially greater enhancement effects arising from mechanical properties and the nanosize tip. Some of the latest research results reveal that a single metal nanocone can guide SPPs and concentrate them effectively at its apex.[17-19] This nanofocused electromagnetic field, localized in nanoscale volume, is helpful to improve the resolution of scanning near-field optical microscopy or spectroscopy. Moreover, by nanofocusing, the intensity of such an electromagnetic field is enhanced by several orders of magnitude, making possible many applications in the fields of surface- or tip-enhanced Raman scattering and molecular fluorescence.[20,21] Also, non-linear optical processes such as second-harmonic generation can be excited, due to the strength of the field near the apex[22,23]. Therefore, the metal nanocone has become a much-studied 3D nanostructure in the nano-optics field due to its special properties.

Incorporating the excellent optical properties of metal nanocone arrays into nanodevices requires simple, rapid and scalable fabrication methods. Among usual top-down fabrication methods, focused ion beam etching and e-beam lithography have been used to create metallic nanostructures with precision, but

Beijing National Laboratory for Condensed Matter Physics, Institute of Physics, Chinese Academy of Sciences, Beijing 100190, P. R. China. E-mail: jjli@iphy.ac.cn; czgu@iphy.ac.cn

fabrication of arrays with these technologies is slow and limited in total obtainable structured area. Similarly, bottom-up approaches that combine colloidal lithography and reactive ion etching are also an alternative, fabricating nanocone arrays by using the colloidal monolayer as an etching mask; however, such processes often require multiple etching steps in order to create the desired nanocone structures.[24,25] Although stamping and nanotransfer printing methods are also reported, it is difficult to fabricate high-density and controllable morphological nanocone array structures.[26-28] In addition, other reported ways of fabricating nanocone arrays, such as shrinking holes and patterned masks, can hardly be performed without complicated technical processes such as multiple lithography or etching.[29,30]

In the present work, we developed a very simple templating approach for fabricating high-density, large-scale metal nanocone arrays. This approach combines the nanoimprint of a hard template of Si nanocones and a replicating technique between soft templates to fabricate a metal nanocone array with a reasonably large area, at low a cost and via a convenient process. To make peeling possible, a crucial baking process is proposed. It depends on the difference between the glass transition temperature (GTT) of the two soft polymer materials that are used to form the deposition template on one hand and the transferring substrate on the other. Using this approach, we have rapidly fabricated a series of metallic nanocone array structures made up of Au, Ag, Al, Ni or Ti nanocones supported on either quartz or Si substrate, demonstrating that the method is universal for producing a variety of metal nanocones. This nanofabrication approach is based solely on template-transfer fabrication without lithography or etching steps. Moreover, this technology is scalable and compatible with standard microfabrication, enabling large-scale production of metallic nanostructures for potential plasmonic optical applications. Further, as-fabricated Au and Ag nanocone arrays are used as SERS substrates for the detection of p-thiocresol molecules, dramatically increasing SERS intensity, with an estimated enhancement factor of $\sim 10^7$.

Experimental Section

Preparation of the initial template. Silicon nanocone arrays are fabricated by inductively coupled plasma (ICP) reactive ion etching technology as a initial hard imprint template, and SF_6 and O_2 are used as etching gas in a cryogenic environment (-120℃). The gas ratio, pressure, power and etching time are four important parameters to control the morphology of Si nanocones (density, height and apex angle). [31] Here, we employ these parameters: gas ratio, SF_6/O_2=22/7; ICP power, 800W; pressure, 6mTorr; and etching time, 7min. In addition, the Si nanocones are coated with an anti-sticking layer by self-assembly before the imprinting process, which is helpful to release the mold from the photoresist. The 1H,1H,2H,2H-perfluorodecyltriethoxysilane (PFDTES) is employed as the anti-sticking layer, and the whole coating process is completed in a pumped glove box. The 0.1ml PFDTES solution is dropped on a silicon wafer next to the substrate covered by as-etched silicon nanocone array and left overnight.

Nanoimprint and metal deposition process. Nanoimprint technology is employed to form conical pits on a soft template by thermal nanoimprint, using a silicon nanocone array as a hard template. The 0.5ml S1813 photoresist (Shipley Series), spin-coated on a silicon or quartz substrate at 3000rpm, is used for the soft template to be imprinted, having ~1.5μm thickness after baking at 115℃ for 1min. The nanoimprinting conditions are controlled as follows: pressure of 20 bar, applied temperature of 60℃ and pressing duration of 4 min. Metal deposition is then accomplished by e-beam evaporation to fill the conical pits in the soft template. The thickness of the resulting metal film is typically about 300nm.

Peeling/transferring process. After the metal filling process**,** the film is simultaneously peeled and transferred. First, 1.5ml SU8 photoresist (MicroChem Corporation) is spin-coated on the Si or quartz substrate at 3000rpm, forming a soft transferring substrate. Second, UV-exposure with a light-intensity of 11mJ/cm^2·s and duration of 90s copolymerizes the SU8 photoresist, and it adheres immediately to the metal surface of the sample. Next, the sandwiched sample is baked at 200℃ for 30 min and then cooled to room temperature. Finally, the sample is reheated to 120℃, and peeling is easily accomplished by mechanical separation. The large-scale metallic nanocone array has thus been transferred to an SU8 soft substrate from the S1813 soft template.

Raman Spectra Measurements. As-fabricated Ag and Au nanocone arrays are immersed in 10^{-4} M p-thiocresol ethanol solution for 2h, and then rinsed with ethanol to get rid of non-adsorbed p-thiocresol molecules. The thiol-group in the molecule is strongly adsorbed on the Au or Ag nanostructure surface through the chemical bounding between the sulfur atom and the gold or silver atom. The SERS of Au and Ag nanocones was

detected by a Raman microscopy system (Renishaw inVia) using a 633nm laser to excite the molecules with 2mW laser intensity.

Results and discussions

A schematic of the fabrication process is shown in Fig.1. Starting from the mold of Si nanocones, conical holes are fabricated in photoresist (S1813) by thermal nanoimprinting. After metal film deposition to fill the holes, the sample is adhered to a second substrate of SU8 thick photoresist, and the metal nanocone array is finished by peeling and transferring after a crucial baking process.

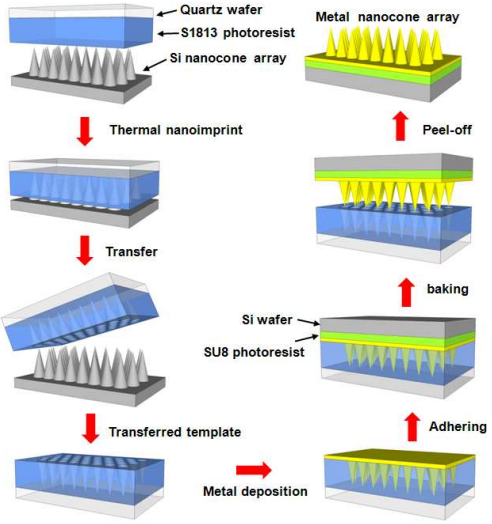

Fig.1 Schematic of the proposed method of metallic nanocone array fabrication: Template nanoimprinting, metal filling, adhesion of second substrate, baking and peeling, along the direction of the red arrows.

Figure 2a shows a typical Si nanocone hard template fabricated by cryogenic etching, with two insets – a random top view of the Si nanocone array and a 4-inch wafer of a Si nanocone array sample. Together, these three images reflect the high density and uniformity of the large-area Si nanocone structure. Figure 2b shows the change in aspect ratio of Si nanocones with etching pressure, showing a controllable geometrical size (3.4~9.8) in the service of the subsequent nanoimprinting process, which demonstrates that control of low etching pressure can tune the aspect ratio of Si nanocones. Among the sample templates of Si nanocone arrays with a density of ~5×10^8 cm^{-1}, the height range of 1.4~2.5 μm and the aspect ratio range of 3.4 ~6.1 can be selected as the nanoimprinted template. We chose S1813 photoresist as nanoimprinting resist because it can be spin-coated up to thicknesses exceeding 1μm and has a relatively low glass transition temperature, two features which are rather important in fabricating metallic nanocones. Figure 2c shows the distribution of imprinted holes on the S1813 soft template after the hot nanoimprinting process, with a density similar to that of the mold of Si nanocones, on which the wavy terrain comes from uneven swarming of the photoresist during thermal imprinting. The height of Si cones is more than twice the thickness of the photoresist to avoid compacting the soft photoresist when it contacts the Si nanocone template. So the depth of an imprinted hole is only the upper half of the corresponding Si cone. Holes that are too deep are unfavorable for the subsequent metal deposition and peeling processes. Next, the metal is deposited into the conical nanoholes by e-beam deposition. Evolution of the surface morphology as the holes are gradually filled with deposited metal is shown in Figure 2c, and we can see that with increasing metal film thickness, the number of holes decreases gradually. Most holes are fully filled when the Au film is built up to about 300nm, but in a few large-diameter holes, the deposited metal still has a small pit. The inset in Figure 2c is a magnified SEM image around a pit showing the distribution of metal particles. Then the upside of the metal film is adhered to a target substrate (transparent or non-transparent substrate), using SU8 resist as the adhesive layer after being cured by UV. In the final step, a crucial heat treatment is controlled to make metal nanocone/SU8 substrate easy to peel off from the S1813 resist, obtaining the finished metallic nanocone array.

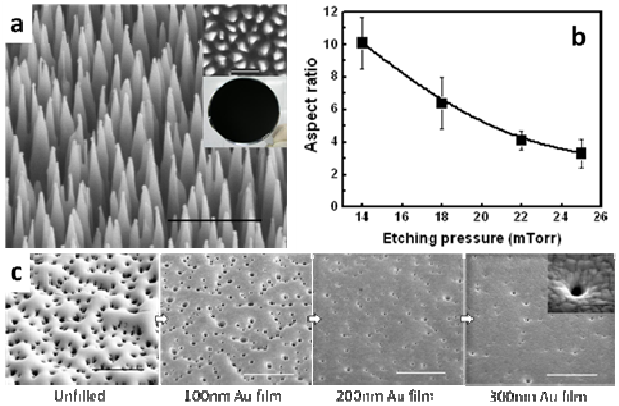

Fig.2 (a) Typical nanoimprinting mold consisting of Si nanocones, with two insets: top view of Si nanocones (scale bar, 2μm) and a wafer-scale sample. (b) Variation of aspect ratio of Si nanocones with etching pressure. (c) Leftmost SEM image shows

photoresist template surface after nanoimprinting and before metal deposition, revealing a large number of conical nanopores. Other SEM images of photoresist surface after metal deposition has reached different film thicknesses are shown (scale bars, 2μm), with most nanopores being covered as film thickess increases. But several large-diameter nanopores are still not fully filled, as shown in an inset. (scale bar, 200nm)

The crucial heat treatment mentioned earlier depends on an important mechanism: when the temperature is far higher than an organic polymer film's intrinsic glass transition temperature (GTT), it will change state from glassy to viscous, and at this moment, the metal nanocones are easily peeled from the softened nanohole template, as shown in Figure 3. In accord with this mechanism, we should select two transferring polymer materials that differ greatly in GTT. The S1813 photoresist has a low GTT of 48℃, so it is easy to break away from the filled metal as the temperature exceeds 48℃ and the S1813 photoresist becomes viscous. On the other hand, a target polymer substrate should have a much higher GTT than S1813 photoresist so that the metallic nanocone array can be transferred to it. High GTT of a high-polymer relies on two factors –high cross-linking density and high molecular weight – so the usual SU8 photoresist is the best candidate, because it is a negative photoresist and chemically amplified photoresist, and the cross-linking density and molecular weight of SU8 both increase after UV-exposure and baking, improving its GTT for the present purpose. Some reported experimental results indicate that the GTT of SU8 can reach 200℃ after proper UV-exposure and baking.[32] Therefore, in preparation for the final and crucial peeling of fabricating metallic nanocone arrays, a UV-exposure process is firstly completed for SU8 coated

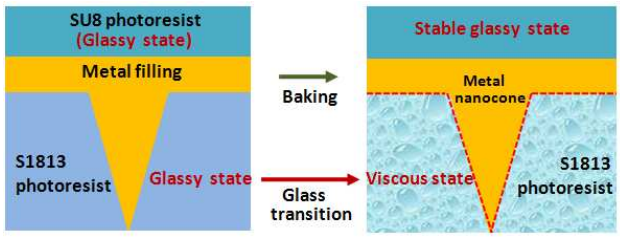

Fig.3 Schematic of the glass transition in S1813 photoresist and the absence thereof in SU8, accounting for the success of this pair of polymer materials. A proper baking process leads to a state transition from glass to viscous in the S1813 template while the SU8 transfer substrate remains in a stable glass state. The difference greatly favors success in peeling the metallic array.

on the target substrate, and then SU8 is adhered immediately to the metal surface of the samples with S1813, which are then baked at 200℃ to enhance the GTT of SU8 and then cooled to room temperature to enhance adhesion to the metal interface. At last, when the samples are reheated to 120℃, S1813 becomes viscous due to the glass transition, but SU8 retains a stable glass state due to its high GTT, and the difference leads to easy mechanical peeling from the S1813 to obtain a metallic nanocone array on the SU8 substrate.

Figure 4 shows a series of metal nanocone arrays fabricated by the above soft-template-peeling method, reflecting good universality for producing nanocones array structures of various metals. Figure 4a is an SEM image of a Au nanocone array with an inset of a single Au nanocone, having a small tip radius of curvature (~20 nm) and an aspect ratio exceeding 2, with a smooth surface. The right-hand optical photographs in Fig.4a show 1cm^2 as-fabricated Au nanocone array samples on quartz and silicon substrates, demonstrating large-scale, highly effective fabrication. Figure 4b ~ 4e show the surface morphology of as-fabricated Ag, Al, Ni, and Ti nanocone arrays, respectively. These as-formed metal nanocones have an aspect ratio range of 2~4 and tip radius of curvature in the range of 20~50 nm.

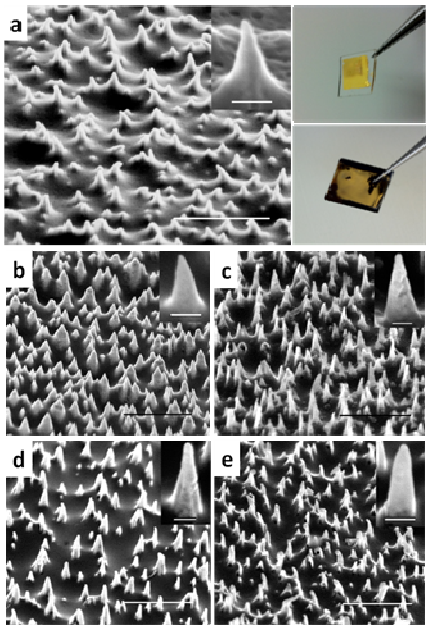

Fig.4 Various as-formed metal nanocone arrays. (a) SEM image of Au nanocone array. The photographs at the right show Au nanocone samples with an area of 1cm^2 on quartz and silicon

substrates. (b)-(e) SEM images of Ag, Al, Ni and Ti nanocone arrays, respectively. Insets show magnified SEM images of corresponding single nanocones. (Scale bars, 2μm for arrays and 200nm for single nanocones.)

Even though the various metal nanocones above originated from the same Si naoncone template, obvious differences in external geometry and size can be observed, which arise mainly from the intrinsic properties of the different metal materials. Different metal materials have different diffusion rates on the photoresist surface during deposition, which dominates the extent to which the nanocone-shaped holes are filled and then determines the tip curvature of the nanocones. In addition, we find two features of as-formed metal nanocones: they are much smaller than the initial Si nanocones, and the surface of some metal nanocone is rough with evident defects. Both are attributed mainly to incomplete filling of imprinted holes during metal deposition, which is related to the metal deposition rate.

Therefore, the metal deposition rate is also an important factor to influence the geometry and surface roughness of metal nanocones. Figure 5 shows the effect of deposition rate on the aspect ratio of Au nanocones, indicating that slow deposition can significantly improve the aspect ratio of Au nanocones. When the deposition rate is lowered to 0.5Å/s for the same imprinted holes, as-formed Au nanocones display a smooth surface with a well defined conical shape and a higher aspect ratio of 2.9, as shown in Fig.5 a. With a faster deposition rate of 1.0 Å/s, the aspect ratio of the Au nanocones is decreased to 2.1 (Fig.5b). When we

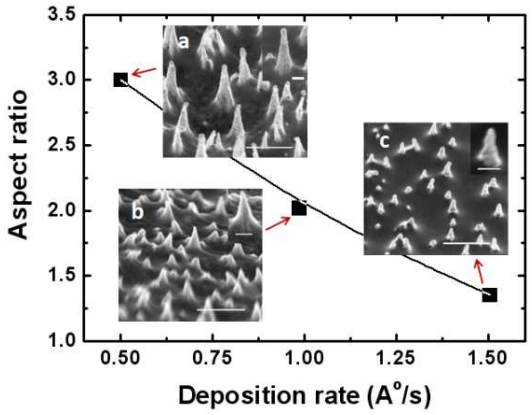

Fig.5 Dependence of aspect ratio of Au nanocones upon deposition rate. Inset SEM images correspond to the morphologies of Au nanocones fabricated at different deposition rates: (a) 0.5Å/s, (b) 1.0Å/s and (c) 1.51.0Å/s. (Scale bars, 1μm for nancone arrays and 200nm for a single nanocones.)

increase the deposition rate further to 1.5 Å/s, the surface of the Au nanocones is rough and the grains of metal are quite apparent, as in the inset of Fig.5c, resulting in an imperfect conical-shape with a low aspect ratio of 1.2. The tip curvature of the metal nanocones can be significantly increased through lowering the metal deposition rate. Under a lower deposition rate, the metal atoms have more time to diffuse on the surface of the photoresist and migrate deep into nanoholes, which is helpful to form smaller metal grains and fill the nanocone-shaped holes for highly conical-shaped structures.

We tried Ag and Au nanocone arrays as SERS substrates and evaluated their performance using p-thiocresol as a model compound, as shown in Fig.6a. The p-thiocresol molecules can be strongly adsorbed on a Au or Ag surface through chemical bonding between sulfur atoms and Au or Ag atoms, which is helpful for a chemical enhancement in SERS detection. In Fig.6a, Ag and Au nanocone array substrates (blue and red curve) give a enhanced Raman signal of adsorbed p-thiocresol molecules, in which the peak intensity for Ag nanocones is 6 times higher than for Au nanocones. The positions of Raman peaks agree well with those in the literature for p-thiocresol on Ag or Au substrate. [33] In contrasting experiments, no SERS spectra are observed for p-thiocresol molecules adsorbed on flat Ag or Au film deposited under the same conditions on glass substrate (green and black curve). The SERS enhancement factor for a Ag nanocone array substrate is estimated to be ~8.2×10^7 using the method described in the literature by comparing the Raman intensity for two peaks at ~1078cm^{-1} and ~1583cm^{-1}. [33] Figure 6b compares as-formed Ag nanocone structures with different cone heights and Ag-coated silicon cone structure, and we can observe that SERS spectral intensity from a Ag-coated silicon nanocone array is weaker than SERS spectral results from a Ag cone structure with high aspect ratio and are comparable to those from a Ag cone structure with low aspect ratio. In addition to obtaining an enhanced Raman signal, two important factors to evaluate the SERS signal are uniformity and repeatability. Figures 6c and 6d show a Raman map across a random 10μm×10μm area of a Ag nanocone array, in which the relative intensity of the two main peaks at 1078 cm^{-1} and 1583 cm^{-1} are mapped using a laser spot diameter of 1 μm and a step-size of 0.3 μm, respectively. Except for very few areas with much stronger or weaker signal, this typical mapping area shows acceptable uniformity with about

10% deviation from the average signal. It should be pointed out that as-measured uniformity may be influenced by a laser spot diameter, and thus this uniformity is used as a reference for SERS detection. Figure 7a shows the repeatability of SERS measurement for the same sample, in which five SERS measurements were completed at 2 hour intervals. Based on the Figure 7a, Figure 7b and 7c display a 2D projected graph and as-subtracted Raman spectra from the first one, respectively, indicating a very small fluctuation of Raman signal which verifies good repeatability. Figure 7d shows the finite-difference time-domain (FDTD) simulation results of the electromagnetic field distribution excited with a laser of 633nm along the XY plane or X=0 section for a single Au nanocone structure on gold substrate with geometric parameters similar to those of a real Au nanocone. It can be seen that the electromagnetic field is mainly bound at the wall-surface of Au nanocone. Along to Y axis direction, the electromagnetic field has a stronger intensity around the nanocone structure, induced by light polarization in the Y direction, as shown in XY plane (left image of Fig.7d). In two enhancement areas along the Z direction (X=0 section, right image of Fig.7d), the field intensity of an enhanced area near at the cone tip is far stronger than that of another area located at the base of the nanocone, indicating an outstanding geometry-enhanced effect, although two enhancement points are out of position on the cone tip, which agrees with some reported results. Previous results show that the greatest SERS enhancement occurs when localized plasmon resonances on the nanostructure's metallic surfaces are present at both the excitation wavelength and the Raman scattering wavelength.[34] So far, the structural parameters of Au or Ag nanocone arrays such as size, separation and height, all of which can greatly affect the plasmon resonances, have not been optimized. Based on our results, it is predicable that the SERS enhancement factor of our nanocone substrate can be further improved by tuning the structure of the templated nanocone arrays to match the optimal SERS requirements.

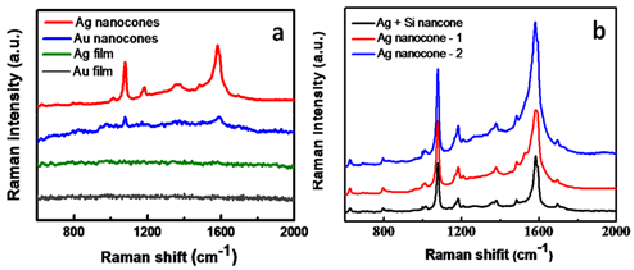

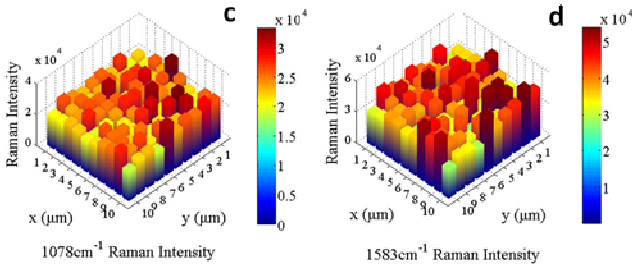

Fig.6 (a) Raman spectra of p-thiocresol molecules adsorbed on four different substrates: Ag, Au nanocones arrays, Ag, Au films, from top down. (b) SERS comparison between as-formed Ag nanocone structure with different cone heights and a Ag-coated silicon cone structure. (c) and (d) Raman maps showing the uniformity of SERS signal across a 10μm×10μm area of a Ag nanocone array. Two main peaks at 1078 cm^{-1} and 1583 cm^{-1} are mapped.

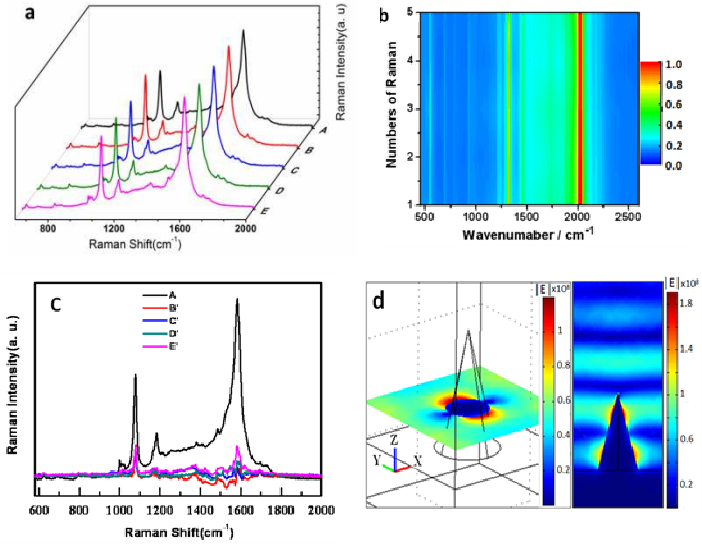

Fig.7 (a) Repeatability measurement of SERS signal in the same sample, including five SERS measurement processes at 2 hour intervals. (b) A 2D projective graph of five plots on (a). (c) as-subtracted Raman spectra, in which four spectra (B',C',D' and E') are subtracted from the first one A. (d) Finite-difference time-domain (FDTD) simulation results of the electromagnetic field distribution excited with a laser of 633nm along the XY plane (Left) and X=0 section (Right) for a single Au nanocone structure on gold substrate; the incident light and its polarization are along the Z axis and Y axis, respectively.

Conclusions

We develop a simple and universal soft-template approach for fabricating large-area metallic nanocone arrays with nano-scale tips and high density. This method combines a nanoimprinting technique and a metal deposition and peeling-off process, but needs no lithography or multiple etching steps, so it is highly efficient and low-cost. A heat treatment process depends on the difference between the GTTs of the two soft substrates to perfectly realize the crucial peeling-off process that exposes the finished metal nanocone array. In addition to shaping the metal nanocones' basic geometry, this method can fine-tune the metal nanocones' morphology in several ways, including size, height, base width, aspect ratio and density, all of which can be modulated by making the nanoimprinting mold properly. In addition, Ag nanocone array structures show good SERS ability with acceptable uniformity and good repeatability. This soft-template peel and transfer technology is scalable and compatible with today's standard microfabrication, enabling mass production of metallic nanocones and also extending this means of fabrication to other metal-array nanostructures, which is promising for a variety of applications such as SERS, field emission, LEDs and other optoelectronic devices.

Acknowledgement

The authors acknowledge the National Natural Science Foundation of China (Grand No. 11174362, 91023041, 91323304, 51272278, 61390503), and the Knowledge Innovation Project of CAS (Grand No. KJCX2-EW-W02).

Reference

1. G. Chen, Y. Wang, M.X. Yang, J. Xu, S. J. Goh, M. Pan, H.Y. Chen, *J. Am. Chem. Soc.*, 2010,**132**, 3644－3645.

2. C. E. Talley, J. B. Jackson,C. Oubre, N. K. Grady, C. W. Hollars, S.M. Lane, T. R. Huser, P. Nordlander, N. J. Halas, *NanoLett.*, 2005, **5**, 1569－1574.

3. Y. Yokota, K. Ueno, H. Misawa, *Small*, 2011, **7**, 252－258.

4. Y.M. Hou, J. Xu, P.W. Wang, D.P .Yu, *Appl. Phys. Lett.*, 2010, **96**, 203107 (3pp)

5. J. Ye, M. Shioi, K. Lodewijks,L. Lagae,T. Kawamura, P. Van Dorpe, *Appl. Phys. Lett.*, 2010, **97**, 163106 (3pp).

6. X.G. Deng, G. B. Braun, S. Liu, P. F. Sciortino Jr., B. Koefer, T. Tombler, M. Moskovits, *NanoLett.*, 2010, **10**, 1780－1786.

7. P. Vasa,R. Pomraenke, S. Schwieger, Y. I. Mazur, V. Kunets, P. Srinivasan, E. Johnson, J. E. Kihm, D. S. Kim, E. Runge, G. Salamo,C. Lienau, *Phys. Rev. Lett.*, 2008, **101**, 116801(4pp).

8. A.Q. Chen, A. E. DePrince III, A. Demortière, A. Joshi-Imre, E. V. Shevchenko, S.K. Gray, U. Welp, V.K. Vlasko-Vlasov, *Small*, 2011, **7**, 2365－2371.

9. F. Le, D. W. Brandl, Y. A. Urzhumov, H. Wang, J. Kundu,N. J. Halas, J. Aizpurua, P. Nordlander, *ACS nano*, 2008, **2**, 707－718.

10. X.D. Ma, H. Tan, T. Kipp, A. Mews, *Nano Lett.*, 2010, **10**, 4166－4174.

11. V. G. Kravets, G. Zoriniants, C. P. Burrows, F. Schedin, A. K. Geim, W. L. Barnes, A. N. Grigorenko, *NanoLett.*, 2010, **10**, 874－879.

12. S.M. Xiao, V. P. Drachev, A.V. Kildishev, X.J. Ni, U. K. Chettiar, H.K .Yuan,V. M. Shalaev, *Nature*, 2010, **466**, 735－738.

13. T. S. Kao, S.D. Jenkins, J. Ruostekoski, N. I. Zheludev, *Phys. Rev. Lett.*,2011, **106**, 085501(4pp).

14. J. Merlein, M. Kahl, A. Zuschlag, A. Sell, A. Aalm, J. Boneberg, P. Leiderer, A. Leitenstorfer, R. Bratschitsch, *Nat. Photon.*, 2008, **2**, 230－233.

15. T. H. Taminiau, F.D. Stefani, F.B. Segerink, N. F. Van Hulst, *Nat. Photon.*, 2008, **2**, 234－237.

16. C. M. Soukoulis, M. Wegener, *Nat. Photon.*, 2011, **5**, 523－530.

17. D. K. Gramotnev, M. W. Vogel, M. I. Stockman, *J. Appl. Phys.*, 2008, **104**, 034311(8pp).

18. M. I. Stockman, *Phys. Rev. Lett.*, 2004, **93**, 137404 (4pp).

19. M. W. Vogel, D. K. Gramotnev, *Phys. Lett. A*, 2007, **363**, 507－511.

20. W.Y. Chang, K.H. Lin, J.T. Wu, S.Y. Yang, K.L. Lee, P.K. Wei, *Micromech. Microeng.*, 2011, **21**, 035023 (5pp).

21. N. A. Issa, R. Guckenberger, *Opt. Exp.*, 2007, **15**, 12131－12144.

22. J. M. Kontio, H. Husu, J. Simonen, M. J. Huttunen, J. Tommila,M. Pessa, M. Kauranen, *Opt. Lett.*, 2009, **34**, 1979－1981.

23. A. Bouhelier, M. Beversluis, A. Hartschuh, L. Novotny, *Phys. Rev. Lett.*, 2003, **90**, 013903 (4pp).

24. M.Toma, G. Loget, R. M. Corn, *Nano Lett.*, 2013, **13**,6164－6169.

25. A. Horrer, C. Schäfer, K. Broch, D.A. Gollmer, J. Rogalski, J. Fulmes, D. Zhang, A.J. Meixner, F. Schreiber, D.P. Kern, M. Fleischer, *Small*, 2013, **9**, 3987－3992.

26. T. I. Kim, J. H. Kim, S. J. Son, S. M. Seo, *Nanotechnology*, 2008, **19** , 295302 (4pp).

27. D. S. Kim, D. H. Kim, J. H. Jang, *Opt. Express*, 2013, **21**, 8450－8459.

28. W. Wu, M. Hu, F. S. Ou, Z. Li, R. S. Williams, *Nanotechnology*, 2010, **21**, 255502.

29. J. M. Kontio, J. Simonen, J. Tommila, M. Pessa, *Microelectron. Eng.*, 2010, **87**, 1711－1715.

30. B. Zeeb, S. Jäger, C. Schäfer, P. Nill, A. J. Meixner, D. P. Kern, M. Fleischer, *J. Vac. Sci. Technol. B*, 2010, **28**, C6O34－C6O37.

31. L. Sainiemi,V. Jokinen, A. Shah, M. Shpak, S. Aura, P. Suvanto, S. Franssila, *Adv. Mater.*, 2011, **23**, 122－126.

32. R. Feng, R. J. Farris, *J. Micromech. Microeng.*, 2003, **13**, 80－88.

33. J.N. Chen, W.S. Yang, K. Dick, K. Deppert, H. Q. Xu, L. Samuelson, H.X. Xu, *Appl. Phys. Lett.*, 2008, **92**, 093110 (3pp).

34. N. J. Halas, S. Lal, W.S. Chang, S. Link, P. Nordlander, *Chem. Rev.*, 2011, **111**, 3913–3961.

A simple and universal soft-template approach is developed for fabricating large-area metallic nanocone arrays with nano-scale tips and high density.